IEEE Access
Multidisciplinary | Rapid Review | Open Access Journal

Received December 10, 2020, accepted December 31, 2020, date of publication January 5, 2021, date of current version January 14, 2021.

Digital Object Identifier 10.1109/ACCESS.2021.3049295

Porous Gold Nanolayer Coated Halide Metal Perovskite-Based Broadband Metamaterial Absorber in the Visible and Near-IR Regime

M. POURMAND, P. K. CHOUDHURY, (Senior Member, IEEE), AND MOHD AMBRI MOHAMMED

Institute of Microengineering and Nanoelectronics, Universiti Kebangsaan Malaysia (UKM) (The National University of Malaysia), Bangi 43600, Malaysia

Corresponding author: P. K. Choudhury (pankaj@ukm.edu.my)

This work was supported in part by the Ministry of Higher Education (MOHE), Malaysia under Grant FRGS/1/2019/STG02/UKM/01/1, and in part by the Universiti Kebangsaan Malaysia, Malaysia under Grant DIP-2019-018.

ABSTRACT Investigation of the optical response of metal-perovskite configuration-based hyperbolic metamaterials (HMMs) was made toward achieving nearly-perfect absorption in the 300–900 nm wavelength span. More precisely, the HMM structure comprised of periodically arranged gold (Au) and methyl ammonium lead iodide ($MAPbI_3$) nanolayers was taken. The results were derived by exploiting the effective medium theory and transfer matrix method. The proposed HMM was found to exhibit nearly-perfect absorption in a regime of 400–800 nm. In order to achieve better uniformity in the wideband absorption, the structure was also modified by replacing the top Au-nanolayer with a porous Au-nanolayer. The analyses of the modified configuration revealed perfect absorption (>99%) for a wide range of incidence angles corresponding to the TM-polarized incidence excitations in the UV and visible regimes. However, the spectra corresponding to the TE-polarized waves exhibited over 70% absorption only. It is expected that this configuration would find potentials in solar energy harvesting, biosensing and active photonic devices.

INDEX TERMS Hyperbolic metamaterials, perovskites, metamaterial absorbers.

I. INTRODUCTION

Subwavelength-sized engineered metal-dielectric nanostructures have been in the research limelight owing to the unique electromagnetic (EM) characteristics [1]–[3]. Such nanoengineered mediums can simultaneously behave as reflector or emissive/absorptive mediums in different operating wavelengths [3]. Within the context, hyperbolic metamaterials (HMMs) are anisotropic in nature, and exhibit hyperbolic dispersion relation. These possess opposite signs for the parallel and perpendicular components of effective permittivity. Varieties of HMMs have been reported in the literature operating in the terahertz (THz) and optical regimes [4], [5] for potential applications in super resolution imaging [1], [6], filtering [7], [8], extreme polarization anisotropy of photo-luminescence [9], energy harvesting [10], biosensors [11], [12], and absorbers [10], [13]–[15].

The associate editor coordinating the review of this manuscript and approving it for publication was Weiren Zhu.

In metamaterials comprising metal-dielectric mediums, the use of metal introduces loss at optical wavelengths, thereby restricting them from versatile usages of such HMMs in this regime [5], [16], [17]. To tackle this problem, one prudent approach remains to incorporate gain mediums as dielectrics in the HMM configuration [16], [18], [19]. Other attempts would be to exploit metal-halide perovskite gain medium in HMMs due to their high refractive index, controllable band-gap, high optical gain, strong nonlinear response, and more importantly, solution processability [17], [20]–[23]. The latter property remains highly desirable for easy integration of perovskite mediums to other optical devices [17], [22].

In the present work, we aim at investigating the HMM structure comprising periodically arranged gold (Au) and solution processable methyl ammonium lead iodide ($MAPbI_3$). We emphasize on achieving enhanced absorption in the 300–900 nm wavelength span corresponding to varying incidence angles of the transverse magnetic (TM) and transverse electric (TE) radiations. We also attempt to obtain the absorption spectra by altering the geometrical properties, namely the filling fraction.

In order to enhance absorption along with the uniformity in the absorption band, we attempt to replace the top Au-nanolayer with a porous Au-nanolayer. It has been reported earlier that porous Au nano-leaf (NAF) exhibits stronger plasmonic properties compared to its bulk counterpart due to the large surface-to-volume ratio [24]–[26]. Moreover, the effective permittivity of NAF can be tailored by altering the pore size and porosity during the fabrication process. Interestingly, the porosity adds more tunability to our proposed HMM configuration. This work paves the way to utilize it in on-chip photonic devices for high-speed light sources, modulators, detectors, biosensors, and more specifically, in energy harvesting solar cells.

This work is organized in a way that, following the introductory part in Section I, Section II provides the design and modelling issues. Section III throws discussions on the proposed metal halide-perovskite-based HMM structure first, and then the porous Au-nanolayer topped HMM configuration is touched upon, stating the comparison aspects of the achieved spectral characteristics. Section IV concludes the obtained results.

II. ANALYTICAL TREATMENT

The EM analyses of materials essentially exploit the constitutive properties, i.e., the permittivity and permeability of mediums, which have to be intelligently derived and used in Maxwell's equations [1], [2], [27]. Within the context, the dispersion relation (or the eigenvalue equation) of anisotropic mediums can be obtained by solving the Maxwell's equations for a plane wave. The tensor form of dielectric permittivity of an isotropic medium, when the optical axis is along the z-direction, is written in Cartesian coordinates as

$$\bar{\bar{\epsilon}}_r = \epsilon_0 \begin{bmatrix} \epsilon_x & 0 & 0 \\ 0 & \epsilon_y & 0 \\ 0 & 0 & \epsilon_z \end{bmatrix} \tag{1}$$

with $\epsilon_x = \epsilon_y = \epsilon_\parallel$ and $\epsilon_z = \epsilon_\perp$. Here ϵ_x, ϵ_y and ϵ_z are, respectively, the x-, y- and z-components of permittivity, along with the subscripts $\parallel$, $\perp$ indicating the parallel and perpendicular components, respectively, of the same. We consider the time-harmonic electric and magnetic components of the incident plane wave of the forms $\bar{E} = E_0 e^{j(\omega t - \bar{k}\cdot\bar{r})}$ and $\bar{H} = H_0 e^{j(\omega t - \bar{k}\bar{r})}$, respectively, where $\bar{k}$ is the wavevector. Under such assumption, the Maxwell's equations can be solved for the electrical field $\bar{E}$ in an isotropic uniaxial medium to get the equation

$$\bar{k}\left(\bar{k}\cdot\bar{E}\right) = \left(|k|^2 - k_0^2\bar{\bar{\epsilon}}_r\right)\bar{E} \tag{2}$$

with k_0 being the wavevector in free-space. After solving the system of equations in Eq. (2), the dispersion relation can be obtained as

$$\left(k_x^2 + k_y^2 + k_z^2 - k_0^2\epsilon_\parallel\right)\left(\frac{k_x^2 + k_y^2}{\epsilon_\perp} + \frac{k_z^2}{\epsilon_\parallel} - k_0^2\right) = 0 \tag{3}$$

where the k_x, k_y and k_z, respectively, represent the x-, y- and z-components of wave vector. The first factor in Eq. (3) associates to the TE-polarization, i.e., $\hat{z}.\bar{E} = 0$, whereas the second factor is related to the TM-polarized waves in which the magnetic field is laid in the xy-plane, i.e., $\hat{z}.\bar{H} = 0$. In the case of $\epsilon_\parallel > 0$ and $\epsilon_\perp < 0$, both the TE and TM modes would exist at the same time – the relevant multilayered stack is designated to be the Type I HMM. On the other hand, when $\epsilon_\parallel < 0$ and $\epsilon_\perp > 0$, the TM mode only exists, and the material is categorized as the Type II HMM.

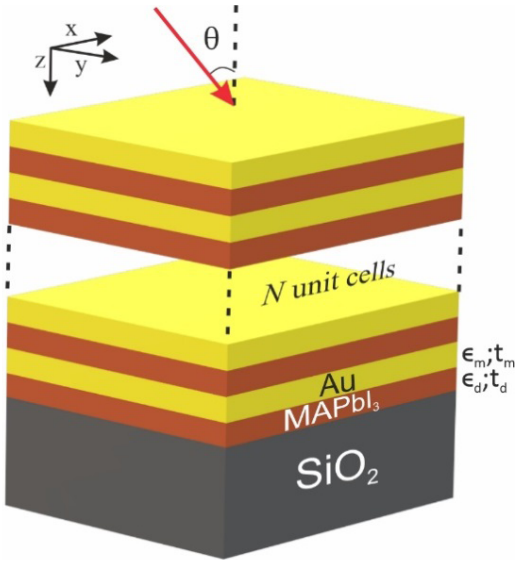

FIGURE 1. Schematic illustration of the proposed perovskite-based HMM absorber.

Keeping in mind the above classification of HMMs, we consider a periodic stack of thin dielectric and metallic layers, as depicted in Fig. 1. In particular, we take a periodic structure comprising $MAPbI_3$ and Au mediums, which the unit cell is comprised of. To be more specific, the overall structure is the organization of 09 unit cells with the bottommost $MAPbI_3$ layer deposited on a relatively thick SiO_2 substrate.

While treating the HMM analytically, if the unit cell is of the subwavelength size (considering the illuminating wavelength), the optical response of HMM can be evaluated by exploiting the effective medium theory (EMT). Within the context, the Maxwell-Garnett approximation can be used to homogenize, which yields the parallel and perpendicular components of permittivity to be of the form [2], [28]

$$\epsilon_\parallel = \rho\epsilon_m + (1-\rho)\,\epsilon_d, \epsilon_\perp = \frac{\epsilon_m\epsilon_d}{\epsilon_d + (1-\rho)\,\epsilon_m} \tag{4}$$

with ρ being the filling fraction of metallic layer, given as $\rho = t_m/(t_m + t_d)$; t_m and t_d, respectively, being the thicknesses of metallic and dielectric layers. Also, in Eq. (4), ϵ_m and ϵ_d represent the permittivity values of metallic and dielectric layers, respectively.

Now, we analyze the HMM structure of Fig. 1 using the transfer matrix method (TMM), which exploits Maxwell's equations, and the propagating waves satisfy the boundary conditions at each layer. Following the technique, the resulting equation can be organized in the form of a 2×2 matrix,

i.e., the transfer matrix M_i, which describes the wave propagation at the ith layer corresponding to the TE and TM modes. We evaluate the total matrix (M_T) as a serial product of each transfer matrix, and is expressed as follows [29]:

$$M_T = \prod_{i=1}^{N} M_i = \begin{bmatrix} m_{11} & m_{12} \\ m_{21} & m_{22} \end{bmatrix},$$
$$M_i = \begin{bmatrix} \cos(k_i t_i) & -\frac{j}{p_i}\sin(k_i t_i) \\ -jp_i \sin(k_i t_i) & \cos(k_i t_i) \end{bmatrix} \quad (5)$$

In these equations, N is the total number of layers used in the composite, m_{ij} represents the transfer matrix components, k_i is the wavenumber (of the normal components), and t_i represents the thickness of each layer. Also, here p_i is determined by the wave polarizations so that it assumes the values either equal to $\left(k_i/\omega\mu_0\right)$ or $\left(k_i/\omega\mu_0\epsilon_0\epsilon_i\right)$, respectively, corresponding to the cases of TE- or TM-polarized incidence excitation. Moreover, μ_0, ϵ_0, are the respective free-space values of permittivity and permeability, and ϵ_i is the parallel component of permittivity of the ith layer.

Now, the absorptivity A for both the polarizations can be obtained from the equation $A(\lambda) = 1 - [T(\lambda) + R(\lambda)]$, where $T(\lambda)$ and $R(\lambda)$ are the wavelength-dependent transmission and reflection coefficients, respectively [29].

III. RESULTS AND DISCUSSION

We now investigate the absorption characteristics of the proposed HMM for different values of filling fraction. In this stream, we first adopt a structure consisting of a unit cell of Au and perovskite ($MAPbI_3$) nanolayers deposited on SiO_2 substrate. We keep the thickness of Au-nanolayer t_m as fixed to 20 nm, whereas that of the perovskite nanolayer is defined by the relation $t_d = t_m(1-\rho)/\rho$, with ρ being the filling fraction. Also, we keep the thickness of the bottom SiO_2 layer fixed as 100 μm. The electrical characteristics of Au, $MAPbI_3$ and SiO_2 are extracted from the experimental results in Refs. [30]–[32].

To fabricate the structure in Fig. 1, the constituent nanolayers (Au, perovskite) would be realized by the layer-by-layer fabrication process. Thin layer of metal can be either sputtered on the SiO_2 substrate or be deposited by e-beam evaporation [17], [24], [26], [33]. Furthermore, the perovskite layer can be realized by using the solvent fabrication process [17], [33]. In this way, the thickness of perovskite layer can be controlled by adjusting the molarity of perovskite solution [17]. Interestingly, the layer thickness of 20 nm to 200 nm can be obtained by exploiting this process.

As stated before in Section II, the investigation of EM behavior of such composites essentially requires the evaluation of effective permittivity. At the first step, we consider an Au-$MAPbI_3$ unit cell with a filling fraction of 0.5, and deduce the real and imaginary parts of permittivity values in a wavelength range of 0.3–1.2 μm. Figures 2a and 2b, respectively, illustrate the wavelength dependence of the real and imaginary parts of the parallel ($\epsilon_\parallel$) and perpendicular ($\epsilon_\perp$) components of effective permittivity for the aforementioned

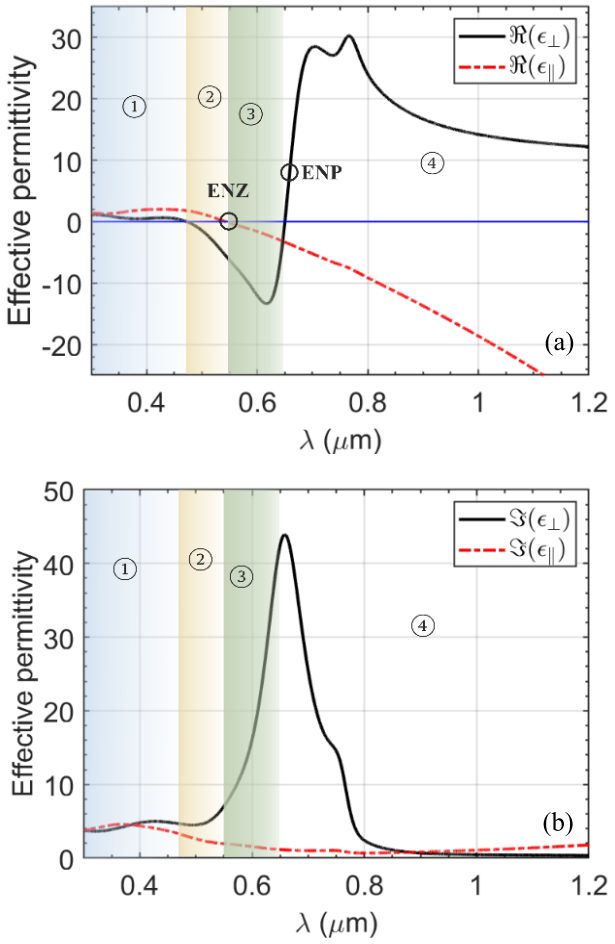

FIGURE 2. Plots of wavelength- (λ-) dependent parallel ($\epsilon_\parallel$) and perpendicular ($\epsilon_\perp$) components of effective permittivity; (a) real parts, (b) imaginary parts.

kind of stack, as deduced upon exploiting the EMT. As can be seen in these figures, we divide the spectral range into four distinct regions, marked by the numbers 1–4 and different colors, based on the $\Re(\epsilon_\perp)$, $\Re(\epsilon_\parallel)$ signs alternations.

We observe in Fig. 2 that, in the first region (the UV window), both the real and imaginary components of effective permittivity exhibit positive values with approximately near free-space properties. The low positive permittivity values allow achieving high impedance matching with free-space, thereby resulting in high absorptivity. Figure 2b depicts that the imaginary parts $\Im(\epsilon_\perp)$, $\Im(\epsilon_\parallel)$ are positive in all regions with $\Im(\epsilon_\perp) > \Im(\epsilon_\parallel)$. Also, up to 0.3 μm, and then over 0.9 μm, these become nearly equal. Figure 2 determines the structure behaving like a very low-loss uniaxial medium in the UV regime. In the second region (i.e., 0.48–0.54 μm), the characteristics of effective permittivity exhibit $\Re(\epsilon_\perp) < 0$, $\Re(\epsilon_\parallel) > 0$, and therefore, the proposed multilayer structure acts as a Type I HMM – the feature that is generally difficult to achieve for multilayered structures, and it promises more transmittivity [17].

Figure 3 exhibits the transmission, reflection and absorption characteristics of the proposed HMM structure in the

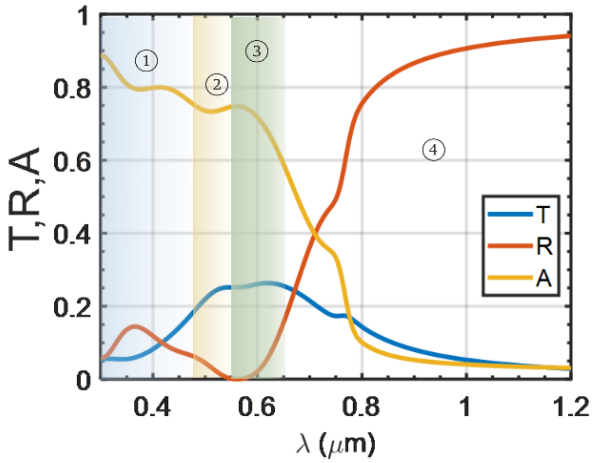

FIGURE 3. Transmission, reflection, and absorption characteristics of the proposed Au/$MAPbI_3$ bilayer stack. The plots are divided into four regions: ① $\Re(\epsilon_\perp) > 0$, $\Re(\epsilon_\parallel) > 0$; ② $\Re(\epsilon_\perp) < 0$, $\Re(\epsilon_\parallel) > 0$ – the Type I hyperbolic medium; ③ $\Re(\epsilon_\perp) < 0$, $\Re(\epsilon_\parallel) < 0$ – the metallic medium; ④ $\Re(\epsilon_\perp) > 0$, $\Re(\epsilon_\parallel) < 0$ – the Type II hyperbolic medium.

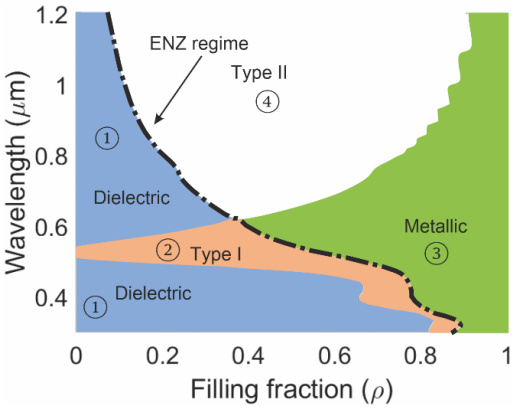

FIGURE 4. Wavelength-dependence of hyperbolic dispersion relation of the proposed multilayer structure corresponding to the different values of filling fraction (ρ). The plots are divided into four regions: ① $\Re(\epsilon_\perp) > 0$, $\Re(\epsilon_\parallel) > 0$; ② $\Re(\epsilon_\perp) < 0$, $\Re(\epsilon_\parallel) > 0$ – the Type I hyperbolic medium; ③ $\Re(\epsilon_\perp) < 0$, $\Re(\epsilon_\parallel) < 0$ – the metallic medium, ④ $\Re(\epsilon_\perp) > 0$, $\Re(\epsilon_\parallel) < 0$ the – Type II hyperbolic medium. The dashed black line indicates the ENZ regime.

0.3–1.2 μm. We clearly observe that the transmittivity rises to higher values in the second region, while the reflectivity reduces to a minimum. The third region starts from the wavelength in which the parallel component of permittivity $\Re(\epsilon_\parallel)$ undergoes epsilon-near-zero (ENZ), as Fig. 2a depicts. The structure exhibits metallic behavior in this region owing to the real components of permittivity being negative, while the imaginary counterparts being positive. Moreover, the real component $\Re(\epsilon_\perp)$ increases sharply in this region 2 from the value –12 at 0.62 μm wavelength, crosses zero at 0.65 μm, and continues to increase to a maximum of +29 at 0.7 μm (Fig. 2a). This clearly shows a kind of singularity in $\epsilon_\perp$, where the constitutive behavior exhibits the perpendicular component of permittivity undergoing a discontinuity in this region. This discontinuity is accompanied with a sharp Lorentzian peak in the imaginary component $\Im(\epsilon_\perp)$ part appearing at 0.66 μm, as Fig. 2b exhibits. The discontinuity is caused by an epsilon-near-pole (ENP) in this region located inside the region 4 with a span of 0.65–1.2 μm. In this region, the proposed structure shows Type II HMM behavior. These are highly reflective, as Fig. 3 depicts. This result clearly shows that the spectral behavior of multilayer structure can be explained by the ENZ and ENP resonance responses [5].

In this work, we emphasize on enhancing the absorption characteristics of the HMM structure. The above results show drop of absorption where the parallel component $\epsilon_\parallel$ of effective permittivity crosses zero, i.e., the ENZ. The longer the ENZ wavelength, the broader the absorption band. As Eq. (4) determines, the $\epsilon_\parallel$-component, and consequently the ENZ, can be defined by changing the Au filling fraction ρ – the property that introduces tunability to the hyperbolic metamaterial structure. As such, we vary the filling fraction ρ in a range of zero (pure $MAPbI_3$) to 01 (pure Au); Fig. 4 exhibits the obtained results in terms of wavelength vs. ρ organizing the different areas according to the signs of $\Re(\epsilon_\perp)$, $\Re(\epsilon_\parallel)$, as Fig. 2 shows. Figure 4 makes it clear that the use of $\rho = 0.375$ yields the maximum hyperbolic dispersion. Furthermore, the ENZ is depicted by a dashed black line in this figure; the maximum absorption band is achievable for the minimum values of filling fraction ρ. As the thickness of metal layer is chosen to be 20 nm and, according to the EMT, the thickness of unit cell must be much less than the wavelength, the minimum value of filling fraction cannot be set smaller than $\rho = 0.2$. As such, we take the value of ρ as 0.2 in our work.

The number of periods used in the fabrication of HMM also remains greatly important to determine the optical properties. As such, we study the effect of the number of periodic Au/$MAPbI_3$ layers on absorption spectra. In such an attempt, we now increase the number of layers N from 1 to 27; Fig. 5 illustrates the obtained results corresponding to the case of $\rho = 0.2$ using the TM-polarized waves with normal incidence excitation. This figure shows that gradual increase in the number of layers leaves trivial impact on the absorption. For $N < 5$, the absorption peak as well as the ENZ regime are mostly affected by resonances caused by the bottom substrate layer. We also observe that the number of layers hardly leaves enough effect on the spectral bandwidth. We see that, for $N > 9$, the absorption peak as well as the ENZ regime are constant, which essentially indicates that further increase in the number of layers hardly leaves significant impact on the absorption properties. It is noteworthy that this property is achieved without implementing a metallic background layer, as used in a previous research report [10].

As stated before, the absorption spectra discussed so far are all obtained for the normal incidence of waves. We now turn to the angular dependency of spectra for the proposed HMM. In this stream, Fig. 6 exhibits the absorption spectra in the 0.3–1.2 μm wavelength span using the obliquity angles of 40° and 80°, and also, with the use of two different numbers of period as $N = 4$ (Fig. 6a) and $N = 9$ (Fig. 6b).

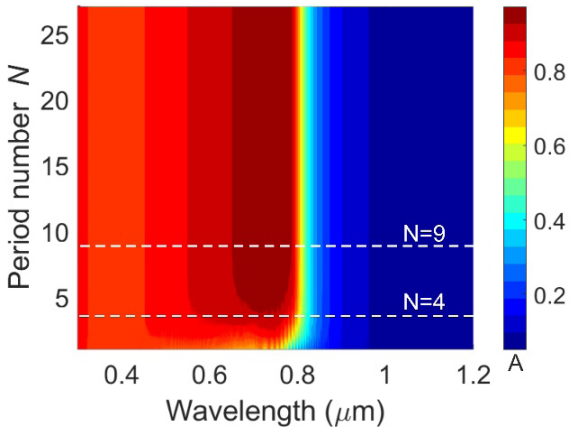

FIGURE 5. Absorption spectra of the proposed nanostructure with different values of N in a range of 1 to 27 corresponding to normal incidence of TM-polarized waves, and the filling fraction as 0.2. The dashed lines indicate two different numbers 4 and 9 of periods.

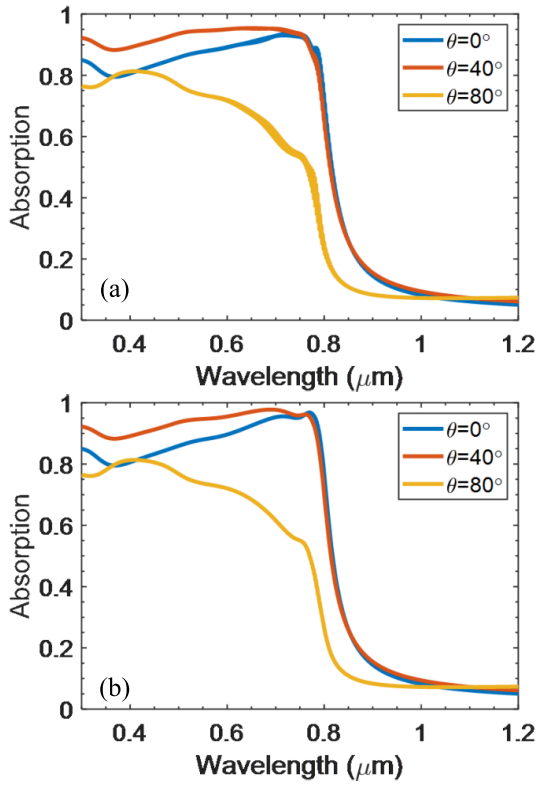

FIGURE 6. Absorption spectra for different values of incidence angle, viz. 0°, 40° and 80° using the number of periods as (a) $N = 4$, and (b) $N = 9$.

For the purpose of comparison, we also include (in Fig. 6) the absorption patterns obtained for the normal incidence of waves. We keep the value of ρ to be 0.2, and all the other operational parameters are left unchanged. We observe in Fig. 6 that the incidence obliquity essentially alters the absorption characteristics. However, the use of 40° obliquity yields the maximum and nearly uniform absorption (of an average of over 96%). Figure 6a shows that, in the case of smaller number of periods N, there are resonances in absorption spectra caused by multiple reflections from the substrate, which decrease upon increasing the number of periods, as Fig. 5b exhibits. Further, the increase in N provides almost near-perfect absorption in the wavelength range of 0.48–0.8 μm (Fig. 6b).

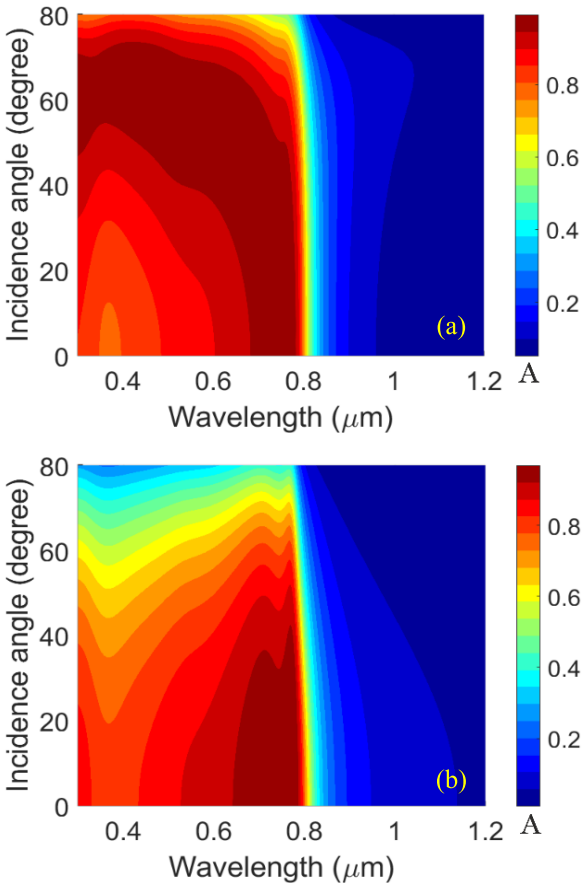

FIGURE 7. Absorption spectra for different values of incidence angle considering the (a) TM, and (b) TE-polarized incidence excitations using $N = 9$.

In order to have a deeper insight into the spectral dependence of absorptivity on the incidence obliquity, we plot the absorption spectra for different angles of incidence ranging from 0°–90°. Figure 7 illustrates the obtained spectral characteristics in the case of $N = 9$ with all the other operating conditions unchanged; this figure includes the situations of TE- (Fig. 7a) and TM- (Fig. 7b) polarized incidence excitations. We clearly notice in Fig. 7 that the absorption spectrum is polarization-insensitive under the normal incidence of waves owing to the symmetry of the proposed structure. However, the absorption spectra corresponding to the TM-polarized excitation are comparably robust in respect of alterations in obliquity; the spectrum maintains the maximum for a wide range of 0°–40° obliquity, and for angles larger than 40°, we observe perfect absorption in the wavelength span of 0.3–0.8 μm, until the incidence angle reaches 75° (Fig. 7a). In contrast, the TE-polarized waves do not exhibit the nature of absorption peaks of the kind the TM waves yield (Fig. 7b). The absorption reduces for the incidence angles larger than 40° due to the presence of pseudo-Brewster angle [17]. A sharp pseudo-Brewster angle

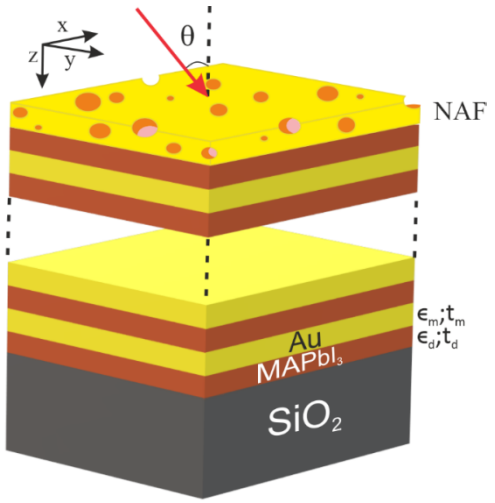

FIGURE 8. Schematic of multilayered Au/$MAPbI_3$ structure with a porous Au NAF at the top.

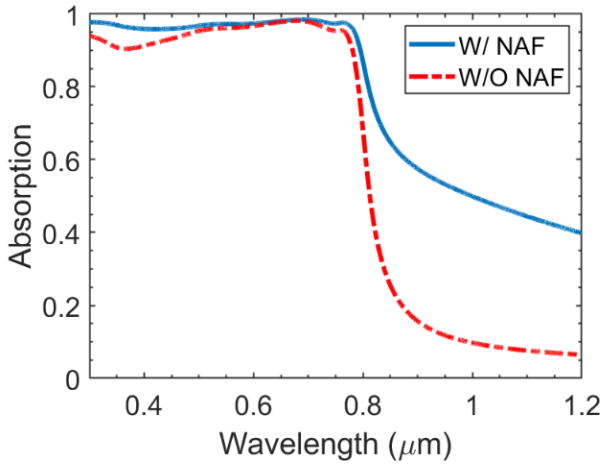

FIGURE 9. Absorption characteristics of the HMM with porous NAF layer (blue solid line) compared to the case of without NAF layer (red dashed line).

allows making tuneable absorbers with polarization selection ability.

As we stated before, the investigation aims at achieving enhanced absorptivity. In order to obtain higher absorption, we attempt to modify the proposed HMM structure by replacing the top Au-nanolayer with a porous NAF layer, as Fig. 8 illustrates. The motivation of this comes from the previously reported study that shows the use of a porous NAF would increase the absorptivity and add tunability to the structure [34]. Such NAF layer can be realized following refs. [24], [26] that determine the electrical properties of the same experimentally.

Figure 9 exhibits the obtained absorption spectra of the multilayered Au/$MAPbI_3$ HMM structure with a porous NAF at the top by exploiting the method of TMM. In this case as well, we take 09 periods of unit cell in total with 08 unit cell periods of Au (solid thin film)/$MAPbI_3$ mounted with 01 period of Au (porous NAF)/$MAPbI_3$; the porous NAF

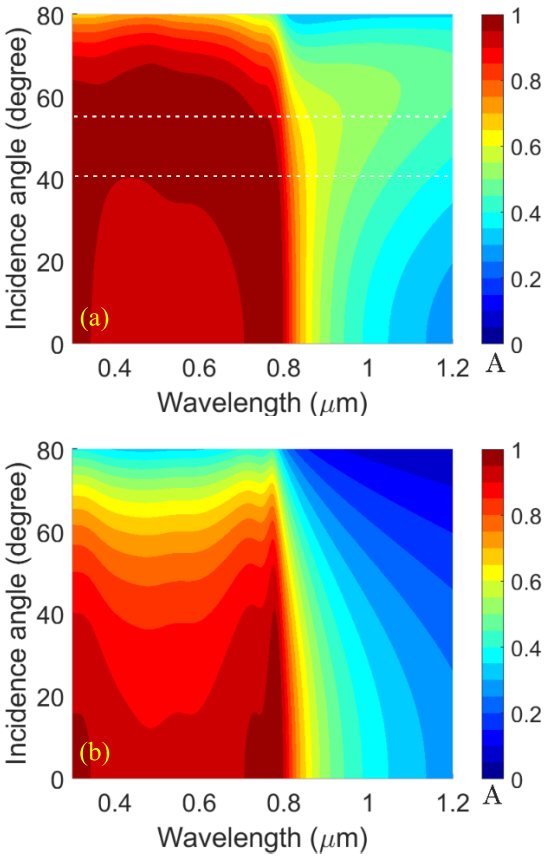

FIGURE 10. Wavelength-dependent absorption spectra for the porous NAF-based HMM corresponding to the (a) TM-, and (b) TE-polarized incidence excitations using different obliquities. The area within two dashed lines represents the perfect absorption regime.

layer at the top being 37.5 nm thick. We illuminate normally the top layer of HMM. Also, we keep the other operating conditions and geometrical parameters the same as used before. Figure 9 clearly determines that the absorption spectra in the UV region are significantly improved upon introducing the porous NAF layer at the top of HMM. It is now more uniform, and also, the absorption is slightly increased corresponding to the wavelength above 800 nm.

To further investigate the effect of porous NAF layer, we retrieve the absorption spectra for the TM- and TE-polarized incidence excitations with different angles of illumination; Figs. 10a and 10b illustrate the obtained results. Figure 10 clearly determines that the newly proposed structure is insensitive to the state of polarization at the normal incidence of waves. Further, corresponding to the case of TM-polarized incidence excitation, the absorption is significantly enhanced in the UV region (Fig. 10a). The absorption spectra remain the same upon reaching 40° obliquity. However, for obliquities in the range of 40°–54.5°, perfect absorption is obtained in the entire UV and visible light regime. In the case of TE-polarized excitation, the pseudo-Brewster angle is visible at 40° (Fig. 10b), where the absorption degrades. In this case, the absorption is not sharp enough as for the structure without the use of porous NAF layer at the top.

IV. CONCLUSION

From the above discussed results, it can be inferred that the optical response of Au/perovskite periodic multilayer configuration in the UV and visible light regime can be understood by exploiting the concept of ENZ and ENP, the positions of which can be governed by suitably controlling the Au filling fraction. Apart from these, the number of periods in the structure also affects the spectral performance; the higher number of periods generally yields relatively higher absorption peaks. However, the results demonstrate that using more than 09 periods of Au/perovskite mediums does not contribute to a better absorption. The incidence obliquity shows that, in the case of TM-polarized excitation, the absorptivity feature would be enhanced to the near-perfect absorption. On the other hand, alterations in absorption spectra are revealed for the TE-polarization due to the pseudo-Brewster angle. The obtained spectral response in the case of incorporating a porous NAF, as created by replacing the top solid Au-nanolayer with a porous Au-nanolayer, shows perfect absorption in the UV and visible light regimes with better uniformity in the wideband response. The results indicate that perfect absorption exists for a large range (40°–54.5°) of incidence obliquity. The achieved results exhibit the device having possible potentials in wideband absorbers, solar cells and energy harvesting applications.

REFERENCES

[1] J. B. Pendry, "Negative refraction makes a perfect lens," *Phys. Rev. Lett.*, vol. 85, no. 18, pp. 3966–3969, Oct. 2000.
[2] D. R. Smith, "Metamaterials and negative refractive index," *Science*, vol. 305, no. 5685, pp. 788–792, Aug. 2004.
[3] A. Alá, M. G. Silveirinha, A. Salandrino, and N. Engheta, "Epsilon-near-zero metamaterials and electromagnetic sources: Tailoring the radiation phase pattern," *Phys. Rev. B, Condens. Matter*, vol. 75, no. 15, Apr. 2007, Art. no. 155410.
[4] V. M. Shalaev, "Optical negative-index metamaterials," *Nature Phys.*, vol. 1, pp. 41–48, Jan. 2007.
[5] P. Shekhar, J. Atkinson, and Z. Jacob, "Hyperbolic metamaterials: Fundamentals and applications," *Nano Converg.*, vol. 1, no. 1, Dec. 2014, Art. no. 14.
[6] Z. Jacob, L. V. Alekseyev, and E. Narimanov, "Optical hyperlens: Far-field imaging beyond the diffraction limit," *Opt. Exp.*, vol. 14, no. 18, pp. 8247–8256, Sep. 2006.
[7] M. A. Baqir and P. K. Choudhury, "Toward filtering aspects of silver nanowire-based hyperbolic metamaterial," *Plasmonics*, vol. 13, no. 6, pp. 2015–2020, Dec. 2018.
[8] M. A. Baqir, P. K. Choudhury, A. Farmani, T. Younas, J. Arshad, A. Mir, and S. Karimi, "Tunable plasmon induced transparency in graphene and hyperbolic metamaterial-based structure," *IEEE Photon. J.*, vol. 11, no. 4, Aug. 2019, Art. no. 4601510.
[9] J. S. T. Smalley, F. Vallini, S. A. Montoya, L. Ferrari, S. Shahin, C. T. Riley, B. Kanté, E. E. Fullerton, Z. Liu, and Y. Fainman, "Luminescent hyperbolic metasurfaces," *Nature Commun.*, vol. 8, no. 1, Apr. 2017, Art. no. 13793.
[10] X. Jiang, T. Wang, Q. Zhong, R. Yan, and X. Huang, "Ultrabroadband light absorption based on photonic topological transitions in hyperbolic metamaterials," *Opt. Exp.*, vol. 28, pp. 705–714, Jan. 2020.
[11] M. E. Nasir, W. Dickson, G. A. Wurtz, W. P. Wardley, and A. V. Zayats, "Hydrogen detected by the naked eye: Optical hydrogen gas sensors based on Core/Shell plasmonic nanorod metamaterials," *Adv. Mater.*, vol. 26, no. 21, pp. 3532–3537, Jun. 2014.
[12] K. V. Sreekanth, P. Mahalakshmi, S. Han, M. S. Mani Rajan, P. K. Choudhury, and R. Singh, "Brewster mode–enhanced sensing with hyperbolic metamaterial," *Adv. Opt. Mater.*, vol. 7, no. 21, Nov. 2019, Art. no. 1900680.
[13] M. A. Baqir and P. K. Choudhury, "Hyperbolic metamaterial-based UV absorber," *IEEE Photon. Technol. Lett.*, vol. 29, no. 18, pp. 1548–1551, Sep. 15, 2017.
[14] M. A. Baqir, P. K. Choudhury, and M. J. Mughal, "Gold nanowires-based hyperbolic metamaterial multiband absorber operating in the visible and near-infrared regimes," *Plasmonics*, vol. 14, no. 2, pp. 485–492, Apr. 2019.
[15] M. A. Baqir and P. K. Choudhury, "Design of hyperbolic metamaterial-based absorber comprised of ti nanospheres," *IEEE Photon. Technol. Lett.*, vol. 31, no. 10, pp. 735–738, May 15, 2019.
[16] Z. Li, J. S. T. Smalley, R. Haroldson, D. Lin, R. Hawkins, A. Gharajeh, J. Moon, J. Hou, C. Zhang, W. Hu, A. Zakhidov, and Q. Gu, "Active perovskite hyperbolic metasurface," *ACS Photon.*, vol. 7, no. 7, pp. 1754–1761, Jul. 2020.
[17] S. Basak, O. Bar-On, and J. Scheuer, "Lead halide perovskite-based active hyperbolic metamaterials in the visible region," *Proc. SPIE*, vol. 11344, Apr. 2020, Art. no. 113441W.
[18] T. Galfsky, H. N. S. Krishnamoorthy, W. Newman, E. E. Narimanov, Z. Jacob, and V. M. Menon, "Active hyperbolic metamaterials: Enhanced spontaneous emission and light extraction," *Optica*, vol. 2, pp. 62–65, Jan. 2015.
[19] L. Lu, R. E. Simpson, and S. K. Valiyaveedu, "Active hyperbolic metamaterials: Progress, materials and design," *J. Opt.*, vol. 20, no. 10, Oct. 2018, Art. no. 103001.
[20] W. Liu, Q. Lin, H. Li, K. Wu, I. Robel, J. M. Pietryga, and V. I. Klimov, "Mn2+-Doped lead halide perovskite nanocrystals with dual-color emission controlled by halide content," *J. Amer. Chem. Soc.*, vol. 138, no. 45, pp. 14954–14961, Nov. 2016.
[21] C.-H. Lee and M.-K. Seo, "Broadband two-dimensional hyperbolic metasurface for on-chip photonic device applications," *Opt. Lett.*, vol. 45, pp. 2502–2505, 2020.
[22] J. You, Z. Hong, Y. Yang, Q. Chen, M. Cai, and T. B. Song, "Low-temperature solution-processed perovskite solar cells with high efficiency and flexibility," *ACS Nano*, vol. 8, pp. 1674–1680, Feb. 2014.
[23] C. Wehrenfennig, G. E. Eperon, M. B. Johnston, H. J. Snaith, and L. M. Herz, "High charge carrier mobilities and lifetimes in organolead trihalide perovskites," *Adv. Mater.*, vol. 26, no. 10, pp. 1584–1589, Mar. 2014.
[24] A. I. Maaroof, A. Gentle, G. B. Smith, and M. B. Cortie, "Bulk and surface plasmons in highly nanoporous gold films," *J. Phys. D, Appl. Phys.*, vol. 40, no. 18, pp. 5675–5682, Sep. 2007.
[25] E. Detsi, E. De Jong, A. Zinchenko, Z. Vukovič, I. Vuković, S. Punzhin, K. Loos, G. ten Brinke, P. R. Onck, and J. T. M. De Hosson, "On the specific surface area of nanoporous materials," *Acta Mater.*, vol. 59, pp. 7488–7497, Dec. 2011.
[26] D. Garoli, E. Calandrini, G. Giovannini, A. Hubarevich, V. Caligiuri, and F. De Angelis, "Nanoporous gold metamaterials for high sensitivity plasmonic sensing," *Nanosc. Horizons*, vol. 4, no. 5, pp. 1153–1157, 2019.
[27] I. Liberal and N. Engheta, "Near-zero refractive index photonics," *Nature Photon.*, vol. 11, no. 3, pp. 149–158, Mar. 2017.
[28] O. Kidwai, S. V. Zhukovsky, and J. E. Sipe, "Effective-medium approach to planar multilayer hyperbolic metamaterials: Strengths and limitations," *Phys. Rev. A, Gen. Phys.*, vol. 85, no. 5, May 2012.
[29] M. Pourmand and P. K. Choudhury, "Wideband THz filtering by graphene-over-dielectric periodic structures with and without MgF_2 defect layer," *IEEE Access*, vol. 8, pp. 137385–137394, 2020.
[30] C. Z. Tan, "Determination of refractive index of silica glass for infrared wavelengths by IR spectroscopy," *J. Non-Crystalline Solids*, vol. 223, nos. 1–2, pp. 158–163, Jan. 1998.
[31] L. J. Phillips, A. M. Rashed, R. E. Treharne, J. Kay, P. Yates, I. Z. Mitrovic, A. Weerakkody, S. Hall, and K. Durose, "Dispersion relation data for methylammonium lead triiodide perovskite deposited on a (100) silicon wafer using a two-step vapour-phase reaction process," *Data Brief*, vol. 5, pp. 926–928, Dec. 2015.
[32] G. Rosenblatt, B. Simkhovich, G. Bartal, and M. Orenstein, "Nonmodal plasmonics: Controlling the forced optical response of nanostructures," *Phys. Rev. X*, vol. 10, no. 1, Mar. 2020, Art. no. 011071.
[33] N. J. Jeon, J. H. Noh, Y. C. Kim, W. S. Yang, S. Ryu, and S. I. Seok, "Solvent engineering for high-performance inorganic-organic hybrid perovskite solar cells," *Nature Mater.*, vol. 13, no. 9, pp. 897–903, 2014.
[34] S. Rout, Z. Qi, M. Biener, D. Courtwright, J. Adrien, M. Shahabuddin, C. E. Bonner, Jr., N. Noginova, and M. A. Noginov, "Tunable optical properties of nanoporous gold leaf metamaterials," *Proc. SPIE*, vol. 11460, Aug. 2020, Art. no. 1146023.

M. POURMAND received the B.Sc. degree in electrical engineering from the Khajeh Nasirodin Toosi University of Technology, Iran, in 2004, and the M.Sc. degree in electrical engineering from the Tafresh University, Iran, in 2013. He is currently pursuing the Ph.D. degree with the Institute of Microengineering and Nanoelectronics, Universiti Kebangsaan Malaysia (The National University of Malaysia), Malaysia. From 2004 to 2020, he worked with the industry sector, as an Electronics Engineer. He has few publications in the following areas. His research interests include the metamaterials, photonic crystals, and plasmonics from fundamental and practical perspectives as well.

P. K. CHOUDHURY (Senior Member, IEEE) received the Ph.D. degree in physics, in 1992. He held academic positions in India, Canada, Japan, and Malaysia. From 2003 to 2009, he was a Professor with the Faculty of Engineering, Multimedia University, Cyberjaya, Malaysia. He was with the Telekom Research & Development (TMR&D), Malaysia, as a Consultant for a couple of projects on optical devices. Thereafter, he joined professorship with the Institute of Microengineering and Nanoelectronics, Universiti Kebangsaan Malaysia, Malaysia. He has published over 250 research articles, contributed chapters to 17 books, and edited and co-edited seven research level books. His research interest includes the theory of optical waveguides, which include complex mediums, fiber optic devices, optical sensors, and metamaterial properties. He is a Senior Member of OSA and SPIE. He is a reviewer for over three dozen research journals. He is also the Section Editor of *Optik–International Journal for Light and Electron Optics* (Elsevier, The Netherlands) and the Editor-in-Chief of the *Journal of Electromagnetic Waves and Applications* (Taylor & Francis, U.K.).

MOHD AMBRI MOHAMMED received the B.E. degree in materials engineering from the Tokyo University of Science, Japan, in 2004, and the M.Sc. and Ph.D. degrees from the Japan Advanced Institute of Science and Technology, Japan, in 2007 and 2010, respectively, both in materials science. He is currently an Associate Professor with the Institute of Microengineering and Nanoelectronics, Universiti Kebangsaan Malaysia (UKM) (The National University of Malaysia). His current research interests include carbon and 2D related materials, and their applications in nanoelectronics devices and epitaxial growth of compound semiconductors.